

### Core Ideas

- The heat ratio method can determine transpiration of larger maize plants.
- Root and leaf simulations are crucial to model transpiration and evapotranspiration.
- Lysimeters are very suitable for model testing.
- Simulations of drought periods and rewet events are challenging.

Helmholtz Zentrum München GmbH, German Research Center for Environmental Health, Institute of Biochemical Plant Pathology, Modelling Plant-Soil Systems, Ingolstädter Landstr. 1, 85764 Neuherberg, Germany. \*Corresponding author (florian.heinlein@helmholtz-muenchen.de).

Vadose Zone J.  
doi:10.2136/vzj2016.05.0042  
Received 12 May 2016.  
Accepted 13 Dec. 2016.  
Open access

Vol. 16, Iss. 1, 2017  
© Soil Science Society of America.  
This is an open access article distributed under the CC BY-NC-ND license (<http://creativecommons.org/licenses/by-nc-nd/4.0/>).

# Evaluation of Simulated Transpiration from Maize Plants on Lysimeters

Florian Heinlein,\* Christian Biernath, Christian Klein, Christoph Thieme, and Eckart Priesack

In central Europe expected climate change will lead to strongly changing regional water availability and will affect future crop production systems and yields. To adapt these production systems and estimate the irrigation necessity for yield optimization—today and in the future—crop water demand as a function of its environment and development stage must be understood. Crop models are often applied to simulate water demands, but the accuracy of the simulations and the underlying mechanisms remain unclear. We therefore grew maize (*Zea mays* L.) in field lysimeters in 2013 and tested the ability of six model configurations (two crop models CERES (Crop Environment Resource Synthesis) and SPASS (Soil-Plant-Atmosphere System Simulation) combined with three evapotranspiration models) to simulate measured sap flow and components of the water balance. Sap flow measurements (i.e., heat ratio method [HRM]) determined transpiration. All models simulated the measured diurnal cycles of sap flow rates. Higher simulated leaf area indices by the CERES model runs caused an overestimation of transpiration in the beginning of the measurement period. The models overestimated daily actual evapotranspiration when water input was high due to an overestimation of actual evaporation and transpiration resulting from high water contents at the top soil layers. All models simulated the occurrence of measured percolation peaks, but only partly captured their intensities. Soil water contents in the 50- and 80-cm depths and the daily water content change of the whole lysimeter were well simulated by the models. Deviations between models and measurements might have been caused by the so-called pot effect and by drought stress influencing the root distribution in the lysimeter.

Abbreviations: ASCE, American Society of Civil Engineers; CERES, Crop Environment Resource Synthesis; DOY, Day of Year; ET, evapotranspiration; HRM, heat ratio method; IA, index of agreement; LAI, leaf area index; NSE, Nash-Sutcliffe model efficiency coefficient; SPASS, Soil-Plant-Atmosphere System Simulation; TDR, time-domain reflectometry.

**Climate change** will have an impact on future growth and yields of agricultural plants. Rosenzweig and Parry (1994) suggested that doubling the atmospheric CO<sub>2</sub> concentration will hardly affect global crop production, but will strongly change regional crop yields. In middle and high latitudes, heat or water stress does not occur, and the effect of increased atmospheric CO<sub>2</sub> concentration on crop growth and yields may outweigh the effect of shorter crop development stages due to higher temperatures. In contrast, at low latitudes the negative effects of shorter growing periods, as well as of heat and water stress on crop yields, can dominate over beneficial direct impacts of higher atmospheric CO<sub>2</sub> concentrations. As a consequence, disparities between more developed countries in temperate climate zones and less developed countries in the subtropical and tropical zones will increase.

In central Europe, expected major aspects of climate change are a shift of precipitation events and amounts toward winter months (Palmer and Räisanen, 2002) and a general increase in extreme events (Beniston et al., 2007), such as heat waves, summer

droughts (Folland et al., 2009), and flash floods (Christensen and Christensen, 2003) during the main growing season in summer.

Milly et al. (2005) expect that by 2050 water availability will increase in high latitude Eurasia and North America and eastern equatorial Africa, but will decrease in southern Europe, southern Africa, the Middle East, and the Midwest of North America. In all regions with declining water availabilities for plant growth during the vegetation period, or where growth is already limited by water availability, plant water use efficiencies may get too low to obtain adequate yields.

To overcome these challenges, irrigation might be a suitable means to address this issue if drainage losses are not too high. Therefore, different irrigation schemes have been tested with lysimeters. Skaggs et al. (2006a,b) measured and simulated root uptake and drainage of different lysimeters planted with alfalfa (*Medicago sativa* L.) and wheatgrass [*Agropyron elongatum* (Host) P. Beauv.]. They applied different irrigation amounts and also changed the salinities of the irrigation water and found that many measured features were captured by the simulations. Phogat et al. (2013) showed that drainage losses can be high, even when the water application is controlled. Their simulations suggest that it is possible to better time fertilization and irrigation to increase plant uptake efficiencies of an orange [*Citrus × sinensis* (L.) Osbeck] crop. Recently, water flow in lysimeters has also been measured by tracer experiments with stable isotopes. Stumpp et al. (2009) observed smaller water fluxes and less drainage when crop rotation was applied in comparison to a maize monoculture. These findings were confirmed during a long-term study that revealed highest drainage and smallest mean transit times of isotopes in a maize lysimeter, while the soil water flow was slower in winter rye (*Secale cereale* L.) and grass cover lysimeters (Stumpp et al., 2012).

Water use of crops and other plants has been measured in different ways. Burgess et al. (2001) used the heat ratio method to measure sap flow in potted *Eucalyptus marginata* Donn ex Sm. trees. Gravimetric measurements and those made with the heat ratio method were closely correlated, also in periods where transpiration rates were low, for example, at night. Further applications of this method were performed on alpine ash (*Eucalyptus delegatensis* R.T. Baker) and snowgum (*Eucalyptus pauciflora* Sieber ex Spreng.) (Buckley et al., 2011), olive trees (*Olea europaea* L.), apple trees (*Malus pumila* Miller), Asian pear trees (*Pyrus* spp.), and grapevines (*Vitis* spp.) (Fernández et al., 2007), various trees and shrubs in California (Fisher et al., 2007), cultivated palms (Madurapperuma et al., 2009), Amazonian trees (Oliveira et al., 2005), and *Eucalyptus vitrix* L.A.S. Johnson & K.D. Hill (Pfautsch et al., 2011).

The heat ratio method in combination with evapotranspiration measurements has also been used to partition evapotranspiration into a soil and a plant component. Er-Raki et al. (2010) showed

that the dual FAO-56 approach gave reasonable estimates of evaporation and transpiration in an olive orchard in central Morocco. They argued that a separate knowledge of these parameters is beneficial to identify soil water stress and to plan irrigation. Herbst et al. (1996) showed the benefits of using different measuring techniques (porometer, lysimeter, and Bowen ratio) to partition reliably between evaporation and transpiration in a maize field in northern Germany and point out the significance of this partitioning for crop yield and water balance estimations. More studies on evapotranspiration partitioning have been conducted by different measurement techniques, such as lysimeters in combination with simulations: Brisson et al. (1998) used the Shuttleworth–Wallace model to simulate transpiration of well-irrigated soybean [*Glycine max* (L.) Merr.] on lysimeters and found highly variable contributions of plants to evapotranspiration. Ding et al. (2013) applied a modified dual crop coefficient model to an irrigated maize field and identified good agreement of the simulations with measured evapotranspiration, evaporation and transpiration from large lysimeter, microlysimeters within the larger lysimeters, and sap flow measurements. In climate simulations, evapotranspiration partitioning also plays an important role by its impact on modeled land–atmosphere interactions. Lawrence et al. (2007) modified the unrealistic evapotranspiration partitioning of the Community Land Model, version 3, toward lower canopy interception and lower evaporation and toward higher transpiration. They found that a higher fraction of transpiration and a lower fraction of interception evaporation led to a weaker but longer lasting evapotranspiration response to a precipitation event as the plants needed more time to take the water up from the soil in comparison to the “direct” evaporation from the leaves. Additionally, this resulted in an increased impact of subsurface soil moisture on transpiration, and hence on the vapor pressure of the atmosphere. Therefore, in the simulations with their model, cloud formation and precipitation were more strongly influenced by the amount of water in the soil.

These findings suggest the importance of identifying a better description of transpiration on the local, regional, and global scales. This includes the mechanistic understanding of root water uptake and plant-internal water transport, as well as dependencies of transpiration on plant development stages, leaf area index, biomass, nutritional status, and crop pests.

The objective of this study was to analyze the components of the simulated water balance of different Expert-N (Priesack et al., 2006; Biernath et al., 2011) model configurations with special focus on the simulation of sap flow. For this purpose, we grew maize plants on a weighing lysimeter and directly measured sap flow in each plant using the heat ratio method, which has often been applied to woody plants, but rarely to herbaceous crop plants like maize. For future applications in the field, we analyzed whether daily transpiration determined by sap flow measurements can be related to daily lysimeter evapotranspiration. Although this setup allows for the determination of the complete water balance,

our focus lies on the directly measured parameters evapotranspiration, transpiration, percolation, and change of soil water content. These quantities were simulated with the modular model framework Expert-N applying six different model configurations, which only varied in the use of three different potential evapotranspiration modules and two different plant growth modules simulating among others leaf and root development. In the next section, the study site, the lysimeter and sap flow measurements, and the different model configurations are presented. Next we compare the results of the model runs with the measurements, including a discussion of the measurements and the different model behaviors. The final section is a summary and conclusion.

## Material and Methods

### Lysimeter Measurements

To measure evapotranspiration (ET) and transpiration (T), maize was sown at a density of 5 plants  $\text{m}^{-2}$  and a sowing depth of 3 cm on 24 Apr. 2013 on two weighing lysimeters at the Helmholtz Zentrum München lysimeter research station near Munich, Germany. Two reference lysimeters lay fallow. All the lysimeters contain 2-m-deep soil columns and have a surface area of 1  $\text{m}^2$ . They are equipped with tensiometers, time-domain reflectometry (TDR) probes, suction cups, and temperature sensors in depths of 50 and 80 cm. No fertilizers were applied during the growing season.

Masses of the lysimeters,  $m_{\text{lysi}}$  [kg], and of the outflow,  $m_{\text{out}}$  [kg] were logged hourly. Weighing precisions of the particular scales were 100 g ( $\hat{=}$  0.1 mm water column) and 10 g ( $\hat{=}$  0.01 mm water column), respectively (Winkler et al., 2009). A more detailed description of the lysimeter facilities can be found in Reth et al. (2007). Soil characteristics of the respective lysimeters are shown in Table 1.

To account for small changes in the calculation of precipitation, which could occur due to wind or presence of animals on the lysimeters, the masses of all four adjoined lysimeters were used for reference. The total masses of each lysimeter system,  $m_{\text{tot}}$  [kg] =  $m_{\text{lysi}} + m_{\text{out}}$ , were calculated. At every hour  $i$   $\Delta m_{\text{tot}}(i) = m_{\text{tot}}(i) - m_{\text{tot}}(i-1)$  was calculated for all four lysimeters. When  $\Delta m_{\text{tot}}(i)$  was smaller than 0.1 kg,  $m_{\text{tot}}(i-1)$  was allotted to  $m_{\text{tot}}(i)$ . By contrast, if all lysimeters showed  $\Delta m_{\text{tot}}(i)$  larger than 0.1 kg, a precipitation event was assumed. Otherwise, precipitation was set to 0 mm. As in temperate climate ET is on average lower than precipitation (in Bavaria: 939 mm yearly precipitation, 517 mm yearly ET), the only constraint of ET to take place, was its occurrence on all four lysimeters:  $\Delta m_{\text{tot}}(i) < 0$ .

### Heat Ratio Method

When stem diameters exceeded 1 cm, heat ratio method (HRM) sap flow devices (ICT International Pty Ltd.) were installed. Sap

Table 1. Soil characteristics of the two lysimeters in this study (Klier, 2007).

| Layer number | Layer depth | Clay | Silt | Sand | Soil type |
|--------------|-------------|------|------|------|-----------|
|              | cm          | %    |      |      |           |
| 1            | 0.0–30.0    | 4.0  | 8.0  | 88.0 | Ss†       |
| 2            | 30.0–50.0   | 4.0  | 8.0  | 88.0 | Ss        |
| 3            | 50.0–80.0   | 3.0  | 5.0  | 92.0 | Ss        |
| 4            | 80.0–200.0  | 1.0  | 1.0  | 98.0 | Ss        |

† Ss denotes very sandy soils with less than 5% clay and 10% silt according to the German soil classification system (Bodenkundliche Kartieranleitung).

flow was measured from 14 August (Day of Year [DOY] 226) to 9 September (DOY 252) 2013.

The HRM sapflow devices use two temperature probes, which are situated 0.5 cm above and below a heating needle. When the heater releases a pulse, the ratio of increase in temperature from initial temperatures  $v_1/v_2$  [ $\text{K K}^{-1}$ ] is measured. This allows for the calculation of the heat pulse velocity  $V_h$  [ $\text{cm h}^{-1}$ ] (Marshall 1958):

$$V_h = k / x \ln(v_1 / v_2) 3600 \quad [1]$$

where  $x$  (0.5 cm) is the distance between the heater and the respective temperature probes and 3600 [ $\text{s h}^{-1}$ ] is a conversion factor. The thermal diffusivity of fresh maize stems  $k$  [ $\text{cm}^2 \text{s}^{-1}$ ] was calculated with the weight and volume of a fresh sapwood sample and its oven-dried weight as suggested by Burgess et al. (2001). The corresponding sap flow software Sap Flow Tool (Version 1.4, ICT International/Phyto-IT) was applied to account for plant and sensor specific impreciseness due to wounding and probe misalignment. These corrections led to an adjusted heat pulse velocity  $V_c$  [ $\text{cm h}^{-1}$ ], which was employed to assess sap velocity  $V_s$  [ $\text{cm h}^{-1}$ ] (Burgess et al., 2001):

$$V_s = \frac{V_c \rho_b (c_w + m_c c_s)}{\rho_s c_s} \quad [2]$$

where  $\rho_b$  (0.162  $\text{g cm}^{-3}$ ) is the measured basic density of stem biomass (dry mass/fresh volume),  $\rho_s$  (1  $\text{g cm}^{-3}$ ) is the density of water,  $c_s$  and  $c_w$  are the specific heat capacities of maize stems (1200  $\text{J kg}^{-1} \text{K}^{-1}$  at 20°C; Becker and Edwards, 1999) and water (sap, 4182  $\text{J kg}^{-1} \text{K}^{-1}$  at 20°C; Lide, 1992), and  $m_c$  (0.811  $\text{kg kg}^{-1}$ ) is the stem water content, calculated as: (fresh weight – dry weight)/fresh weight.

Single outliers within the raw data were neglected if  $V_h$  exceeded threshold values of 60  $\text{cm h}^{-1}$ . The zero base line of the data was determined by sap flow at senescence, where sapflow was assumed to approach zero. To account for small variations and to better

compare with model results hourly averages of sap velocities were calculated. Furthermore, the hourly sap velocities of all plants were multiplied with the corresponding xylem areas, summed up, and divided by the lysimeter area to obtain the lysimeter transpiration [ $\text{mm h}^{-1}$ ].

## Model Setup

We performed the presented simulations using the Expert-N model system, version 5.0 revision 598 (in the following Expert-N refers to this version if not otherwise marked) with an hourly time step. In this study, the model was driven by 1-h resolution weather data from the meteorological station in Garching, which is 4 km away from the lysimeter site and operated by the Meteorologisches Institut München, Germany.

Using Expert-N (Priesack et al., 2006; Biernath et al., 2011), we applied the hydraulic function and pedotransfer functions as suggested by van Genuchten (1980) and Mualem (1976), and Campbell (1986), respectively. In a first step, we estimated soil hydraulic parameters using the ROSETTA software, version 1.2 (Schaap et al., 2001). In a second step, porosities, wilting points, residual water contents, van Genuchten parameters, and hydraulic conductivities of the different layers were adjusted to account for changing soil properties compared to 2007 and to better match the water content measurements in the 50- and 80-cm depths. These parameters are shown in Table 2.

Three approaches were used to simulate potential evapotranspiration,  $\text{ET}_{\text{pot}}$  [mm]. The Penman Monteith approach as proposed by the American Society of Civil Engineers (ASCE) (Walter et al., 2005) is able to simulate different potential evapotranspiration rates during arbitrarily small time steps:

$$\text{ET}_{\text{pot}} = 24 \frac{1/L_{\text{evap}} \Delta(R_n - G) + \gamma C_n / (T_{\text{air}} + 273) u_2 (e_s - e_a)}{\Delta + \gamma(1 + C_d u_2)} \quad [3]$$

where 24 [ $\text{h d}^{-1}$ ] is a conversion factor,  $L_{\text{evap}}$  [ $\text{MJ m}^{-2} \text{mm}^{-1}$ ] the latent heat for condensation of water,  $\Delta$  [ $\text{kPa } ^\circ\text{C}^{-1}$ ] the slope of the saturation vapor pressure-temperature curve,  $R_n$  [ $\text{MJ m}^{-2} \text{h}^{-1}$ ] the calculated net radiation at the crop surface,  $G$  [ $\text{MJ m}^{-2} \text{h}^{-1}$ ] the soil heat flux density at the soil surface,  $\gamma$  [ $\text{kPa } ^\circ\text{C}^{-1}$ ] the psychrometric constant,  $C_n$  ( $37 \text{ K mm s}^3 \text{ Mg}^{-1} \text{ h}^{-1}$ ) the numerator

constant, which depends on reference type and calculation time step,  $T_{\text{air}}$  [ $^\circ\text{C}$ ] the actual air temperature,  $u_2$  [ $\text{m s}^{-1}$ ] the wind speed at the 2-m height,  $e_s$  [ $\text{kPa}$ ] the saturation vapor pressure,  $e_a$  [ $\text{kPa}$ ] the actual vapor pressure, and  $C_d$  (at daytime  $0.24 \text{ s m}^{-1}$  and at nighttime  $0.96 \text{ s m}^{-1}$ ) the denominator constant, which depends on reference type and calculation time step. Besides the direct influence of measured temperature, wind speed and radiation on  $\text{ET}_{\text{pot}}$ , relative humidity is required for the calculation of  $e_a$ . Soil heat fluxes, which become particularly important when hourly ET is calculated, were computed using a partial differential equation to represent soil heat transfer (Hansen et al., 1990). This approach considers the volumetric heat capacity [ $\text{J m}^{-3} ^\circ\text{C}^{-1}$ ] and the thermal conductivity [ $\text{J m}^{-1} \text{d}^{-1} ^\circ\text{C}^{-1}$ ] of the soil according to de Vries (1952, 1963) including the volumetric flow [ $\text{m d}^{-1}$ ] and the specific heat capacity [ $\text{J kg}^{-1} ^\circ\text{C}^{-1}$ ] of soil water.

The approach as suggested by FAO (Allen et al., 1998) was applied with daily time steps. In this case, Eq. [3] is also valid, but  $C_n$  ( $900 \text{ K mm s}^3 \text{ Mg}^{-1} \text{ h}^{-1}$ ) and  $C_d$  ( $0.34 \text{ s m}^{-1}$ ) take different values when a daily time step is employed. Additionally, daily radiation sums and daily averages of temperature, wind speed and relative humidity are used as input, while the calculation of daily actual and saturation vapor pressure incorporates daily maximum and minimum temperatures.

The simplest approach applied is the one of Haude (1955) using the difference of saturation vapor pressure and vapor pressure at 14:30 CET. Thus, only air temperature  $T_{\text{air}}$  [ $^\circ\text{C}$ ] and relative humidity RH [%] at the 2-m height at this time are required as model input variables:

$$\text{ET}_{\text{pot}} = f_{\text{Haude}} (e_s - e_a) = f_{\text{Haude}} (1 - \text{RH}/100) 6.11 \exp[17.269 T_{\text{air}} / (237.3 + T_{\text{air}})] \quad [4]$$

where  $f_{\text{Haude}}$  is the Haude factor, which depends on the crop and on the month. These Haude factors were originally derived for the specific climatic conditions in Germany.

For all three approaches,  $k_c$  factors of 0.3 (initial), 0.8 (midseason), and 0.35 (end of the late season) depending on the plants' phenological development stages were assumed. In contrast, the FAO (Allen et al., 1998) suggests a maximum  $k_c$  factor of up to 1.2 for maize to calculate an upper boundary of crop ET. However, this

Table 2. Estimated soil hydraulic parameters.

| Layer number | Layer depth | Saturated water content           | Residual water content | Hydraulic conductivity | van Genuchten $\alpha$ | van Genuchten $n$ |
|--------------|-------------|-----------------------------------|------------------------|------------------------|------------------------|-------------------|
|              | cm          | — $\text{cm}^3 \text{ cm}^{-3}$ — |                        | $\text{cm d}^{-1}$     | $\text{cm}^{-1}$       |                   |
| 1            | 0.0–30.0    | 0.388                             | 0.157                  | 500.0                  | 0.0365                 | 1.2109            |
| 2            | 30.0–50.0   | 0.388                             | 0.157                  | 500.0                  | 0.0365                 | 1.2109            |
| 3            | 50.0–80.0   | 0.388                             | 0.160                  | 720.0                  | 0.034                  | 1.4669            |
| 4            | 80.0–200.0  | 0.366                             | 0.154                  | 1390.0                 | 0.0309                 | 1.8806            |

is only valid when there are no limitations due to water availability, low plant densities or diseases. Since in our study the plant density was only 5 plants per  $m^2$ , while plant densities in the fields typically tend to be higher (up to 10 plants per  $m^2$ ), this limitation was recognized by a lower  $k_c$  factor. To facilitate interactions with other parts of the model system, daily evapotranspiration rates simulated by FAO and Haude were distributed over each day from 7:12 to 19:12 using a cosine function depending on the time of the day (Childs and Hanks 1975).

$ET_{pot}$  comprises potential evaporation,  $E_{pot}$  [mm], and potential transpiration,  $T_{pot}$  [mm], which are given by:

$$E_{pot} = [1 - SCF(LAI)]ET_{pot} \quad [5]$$

$$T_{pot} = ET_{pot} - E_{pot} \quad [6]$$

The soil cover fraction (SCF) was calculated as leaf area index (LAI)/3. Other soil cover was neglected. This means that the partitioning of ET is identical among the different models when the same LAI value is simulated.

Actual evaporation,  $E_{act}$  [mm], is determined as the minimum of potential evaporation  $E_{pot}$  and the maximal evaporative flux calculated by solving the Richards equation (Nimah and Hanks, 1973). Soil water fluxes were simulated by applying the approach of the HYDRUS model (Šimůnek et al., 1998) as implemented in Expert-N to numerically solve a mixed form of the Richards equation (Richards, 1931) assuming the “free drainage” lower boundary condition.

Plant growth was simulated with the crop canopy models CERES (Ritchie, 1991; Godwin and Jones, 1991; Jones and Kiniry, 1986; Ritchie et al., 1987; Ritchie and Godwin, 1989) and SPASS (Wang, 1997; Wang and Engel, 1998, 2000; Gayler et al., 2002). These models simulate crop phenology, root and leaf development, photosynthesis, nitrogen demand and uptake, biomass growth, potential and actual transpiration, and senescence.

CERES and SPASS apply a similar approach to simulate actual transpiration,  $T_{act}$  [mm]: At first, the maximum water uptake rate of the plant depending on its development stage is calculated. Then the potential root water uptake per soil layer is computed. This parameter depends on the difference between actual water content and the wilting point of the soil layer, as well as on the root length density in this specific layer. The potential root water uptake per soil layer (limited by the maximum water uptake rate) is summed up as maximum total root water uptake, TRWU [mm], and compared to  $T_{pot}$ . If  $T_{pot}$  is lower than TRWU, TRWU will be reduced. This reduction of root water uptake is then equally partitioned to all rooted soil layers. Additionally, if the soil water

content became lower than the wilting point in a certain soil layer, the water uptake from this layer would be further limited and hence also  $T_{act}$ . While CERES calculates a daily  $T_{act}$ , which is then distributed over the whole day from 7:12 to 19:12 using a cosine function (Childs and Hanks, 1975), SPASS computes transpiration rates at every time step. Finally, actual evapotranspiration,  $ET_{act}$  [mm], is calculated as sum of  $E_{act}$  and  $T_{act}$ . Additionally, to convert simulated transpiration into simulated sap flow, transpiration is multiplied by a conversion factor taking the lysimeter area and the cross-sectional areas of conducting sapwood into account.

However, there are further differences between the CERES and SPASS approaches. CERES was run with a module-internal daily time step, while in Expert-N version 5.0 the SPASS crop growth model was modified for application with arbitrarily small time steps. In other words, the SPASS module is called at every time step and thus directly accounts for diurnal variations of water flux, which facilitates immediate interactions with other parts of the model system. The CERES approach distinguishes among nine phenological development stages finishing at distinct points in time: sowing, germination, emergence, end of juvenile phase, tassel initiation, 75% silking, start of the grain-filling phase, end of the grain-filling phase, and physiological maturity. SPASS uses three main phases: the phase before emergence, the vegetative, and the generative phase. CERES emanates from a “big leaf” assumption to simulate light interception and relates biomass production empirically to the calculated light use efficiency. By contrast, SPASS simulates a gross photosynthesis rate using a light saturation curve. The calculation of light interception considers plant height, daylength and shadowing of leaves. To simulate biomass growth CERES partitions assimilates with a variety specific priority scheme depending on phenological development, and water and nitrogen availability. In SPASS, the simulated N concentrations of the different plant compartments affect the user-defined assimilate partitioning. In both approaches, the root growth models are similar and depend on soil temperature, soil moisture, and soil N concentration. However, root length density growth differs due to different schemes of assimilate partitioning influencing the respective growth rate. Senescence occurs in both models when shadowing is higher than a critical value, but the models differ in the mortality rates and the dependencies on the phenological development stage. The complete Expert-N model configuration, which was used for the simulations, is shown in Table 3.

## Data Analysis

We compared the simulated sap flow rates and other components of the lysimeter water balance with the respective measurements using the Index of Agreement (IA, Willmott 1981) and the Nash-Sutcliffe model efficiency coefficient (NSE, Nash and Sutcliffe 1970):

$$IA = 1 - \frac{\sum_{i=1}^N (P_i - O_i)^2}{\sum_{i=1}^N (|P_i - \bar{O}| + |O_i - \bar{O}|)^2} \quad [7]$$

Table 3. The Expert-N model configuration. The different potential evapotranspiration as well as the different plant growth and transpiration modules were combined to generate the six different model configurations; the other submodules were the same in every model configuration.

| Submodule(s) of Expert-N                       | Name   | Reference   |
|--|--|---|
| Pedotransfer functions                         | Campbell   | Campbell (1986)   |
| Hydraulic functions                            | van Genuchten and Mualem                             | van Genuchten (1980), Mualem (1976)   |
| Water flow module                              | HYDRUS   | Šimůnek et al. (1998)   |
| Soil heat transfer                             | DAISY  | Hansen et al. (1990)  |
| Soil nitrogen transport                        | ADE LEACHN   | Hutson and Wagenet (1992)   |
| Nitrification, denitrification, mineralization | CENTURY_N  | Parton et al. (1994)  |
| Potential evapotranspiration                   | Penman Monteith ASCE<br>Penman Monteith FAO<br>Haude | Walter et al. (2005)<br>Allen et al. (1998)<br>Haude (1955)   |
| Plant growth and transpiration                 | SPASS<br>CERES                                       | Wang (1997), Wang and Engel (1998), 2000), Gayler et al. (2002)<br>Ritchie (1991), Godwin and Jones (1991), Jones and Kiniry (1986), Ritchie et al. (1987), Ritchie and Godwin (1989) |

$$NSE = 1 - \frac{\sum_{i=1}^N (P_i - O_i)^2}{\sum_{i=1}^N (O_i - \bar{O})^2} \quad [8]$$

where  $P_i$  and  $O_i$  are prediction and observation at a certain point in time  $i$ ,  $\bar{O}$  the average of all observations, and  $N$  the number of pairs of variates. The IA has an upper bound of 1, which is reached when all  $P_i$  and  $O_i$  are equal. This means a perfect match of prediction and observation. The lower bound of IA is 0. In this case, all the  $P_i$  might be equal to  $\bar{O}$  or  $P_i$  and  $O_i$  might be completely out of phase:  $P_i - \bar{O} = -(O_i - \bar{O})$ . The NSE is in the range between  $-\infty$  and 1. When the NSE is 1, prediction and observation match perfectly. The simulation is as accurate as the mean of the observation when the NSE is 0. Consequently, when the NSE is lower than 0, the average of the observation better predicts the observed values than the simulation.

## Results and Discussion

### Weather Data

Figure 1 shows the measured weather conditions during the sap flow measurement period from 14 Aug. (DOY 226) to 9 Sept. (DOY 252) 2013. Maximum net radiation was  $850 \text{ W m}^{-2}$  on cloud-free days, while lower daily maxima ( $\sim 250 \text{ W m}^{-2}$ ) occurred on cloudy days. Temperature, in general, behaved in a similar manner than radiation. Daily maximum temperatures were up to almost  $30^\circ\text{C}$  high, and the minimum temperature in the analyzed period was  $8^\circ\text{C}$ . High maximum temperatures were observed on days with a high amount of incoming radiation. These days were characterized by daily temperature amplitudes of more than  $15^\circ\text{C}$ . By contrast, on cloudy days daily temperature amplitudes were low. Measured precipitation was also consistent

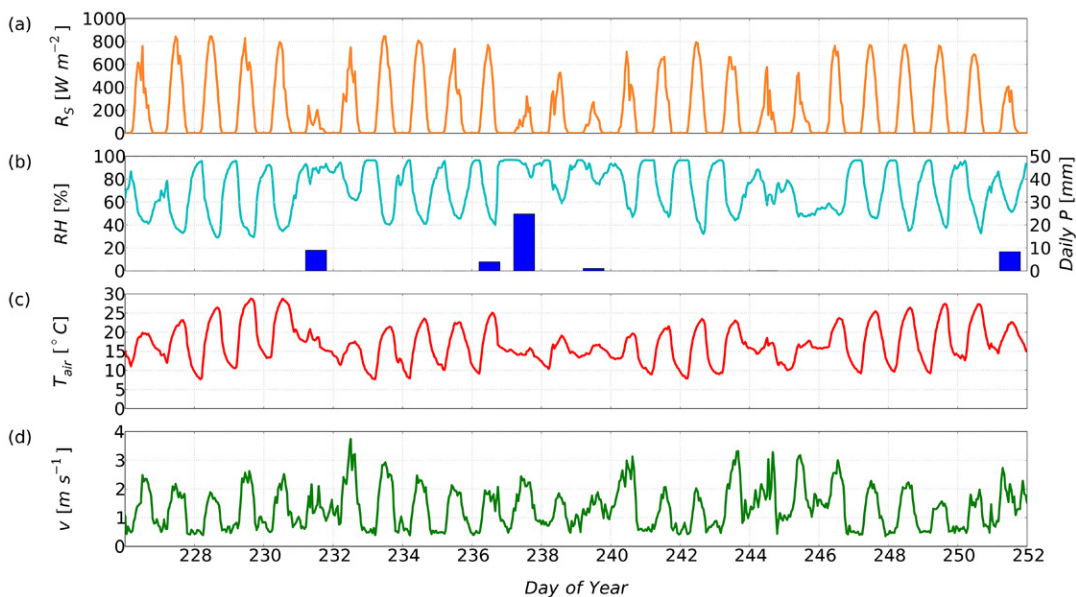


Fig. 1. Time series of measured weather data from 14 Aug. to 9 Sept. 2013: (a)  $R_s$  is the global radiation [ $\text{W m}^{-2}$ ], (b, left y axis) RH is the relative humidity [%], (b, right y axis) daily P the daily precipitation [mm], (c)  $T_{\text{air}}$  the air temperature [ $^\circ\text{C}$ ] and (d)  $v$  the wind speed [ $\text{m s}^{-1}$ ] in the 2-m height.

with radiation measurements. The major precipitation (25 mm  $d^{-1}$ ) occurred on 25 Aug. (DOY 237). Precipitation (up to 10 mm  $d^{-1}$ ) was also registered on 19, 24, and 27 Aug. and 8 Sept. (DOY 231, 236, 239, and 251) 2013. Relative humidity was characterized by diurnal cycles and reached minimum values of 35% during the day and maximum values of 95% at night. On rainy days relative humidity was rarely lower than 80% and was clearly related to temperatures and radiation. As a result of high temperatures and incoming solar radiation, turbulence occurred during the day, leading to wind speeds of up to 3.8 m  $s^{-1}$ . In the afternoons, temperatures and radiation decreased and the near surface atmospheric boundary layer started to decouple from the rest of the atmosphere. This impeded turbulence, and thus, wind speeds tended to be lower than 1 m  $s^{-1}$  until the next morning.

### Sap Flow Measurements and Transpiration Simulations

Figure 2 shows modeled and measured sap flow rates from 14 Aug. (DOY 226) to 9 Sept. (DOY 252) 2013. The measured sap flow rates differed among the plants, but showed similar dynamics. Distinct diurnal cycles were observed in the periods until 18 Aug. (DOY 230), from 20 to 24 Aug. (DOY 232–236), on 26 Aug. (DOY 238) and from 28 Aug. (DOY 240) 2013. This finding is in agreement with the measured weather data of these periods, which showed high diurnal variations of net radiation, temperature and relative humidity. By contrast, on 19, 25, and 27 Aug. (DOY 231, 237, and 239) 2013, maximum sap flow rates were low, not exceeding 45 mm  $h^{-1}$ . All these 3 d were characterized by small daily temperature amplitudes, low maximum net radiation, and high relative humidity. Additionally, precipitation was registered on these days. However, precipitation did not necessarily prevent sap flow. For instance, on 24 Aug. (DOY 236) and 8 Sept. (DOY 251) 2013, diurnal cycles of sap flow rates with maximum values of 180 and 105 mm  $h^{-1}$  were observed despite the occurrence of rain. Accordingly, sap flow rates were controlled by fluctuating temperature, radiation, and relative humidity rather than by rain.

On 18 Aug. (DOY 230) 2013, the highest averaged sap flow during the analyzed period (200 mm  $h^{-1}$ ) was observed. In general, daily maximum sap flow rates of the different plants diverged from each other. The largest difference of daily maximum sap flow rates of two plants occurred on 15 Aug. (DOY 227) 2013 when one plant's maximum sap flow rate was 118 mm  $h^{-1}$  and another was 325 mm  $h^{-1}$ . During most of the time, there was one plant that clearly transpired more than the other plants and one plant that transpired least. Possible reasons for deviations in measured sap flow rates among the individual plants were different stem thicknesses, which are related to different xylem sizes, different leaf areas, different rooting depths, different exposure to solar radiation of each individual plant, and horizontal divergence of soil water contents. During nighttime, small sap flow rates (up to 20 mm  $h^{-1}$ ) were measured. Daily transpiration determined by sap flow measurements was generally of the same order of magnitude as lysimeter ET, but between 20 and 50% lower.

The simulations of sap flow derived from transpiration simulated by the SPASS and CERES crop models also showed distinct, but differently developed diurnal cycles depending on the choice of the potential evapotranspiration model. Maximum potential sap flow rates (not shown) in the analyzed period were about 190 mm  $h^{-1}$  ( $ET_{ASCE}$ , SPASS), 215 mm  $h^{-1}$  ( $ET_{ASCE}$ , CERES), 175 mm  $h^{-1}$  ( $ET_{FAO}$ , SPASS), 185 mm  $h^{-1}$  ( $ET_{FAO}$ , CERES), 255 mm  $h^{-1}$  ( $ET_{Haude}$ , SPASS), and 285 mm  $h^{-1}$  ( $ET_{Haude}$ , CERES). During daytime, from 14 to 18 Aug. (DOY 226–230) 2013, all SPASS simulations showed minor water stress (up to 19 h,  $ET_{Haude}$ , SPASS). Then the potential sap flow rates were higher than the actual sap flow rates. That means the simulated plants would have transpired more if more water could have been taken up by the plants from the rooted soil layers. On the other days, potential and actual sap flow rates were the same. Maximum actual sap flow rates amount to 182 mm  $h^{-1}$  ( $ET_{ASCE}$ , SPASS), 215 mm  $h^{-1}$  ( $ET_{ASCE}$ , CERES), 175 mm  $h^{-1}$  ( $ET_{FAO}$ , SPASS), 185 mm  $h^{-1}$  ( $ET_{FAO}$ , CERES), 190 mm  $h^{-1}$  ( $ET_{Haude}$ , SPASS) and 285 mm  $h^{-1}$  ( $ET_{Haude}$ , CERES).

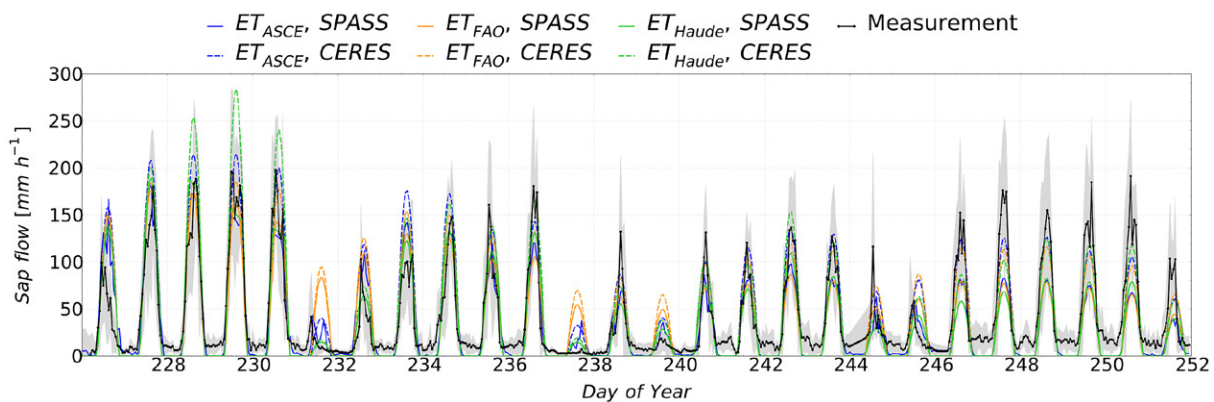


Fig. 2. Time series of measured and simulated sap flow rates from 14 Aug. to 9 Sept. 2013. The measured values (solid black line with dots) are hourly averaged means of sap flow rates [ $mm h^{-1}$ ] from five different maize plants on one lysimeter and comprise standard deviations (gray shaded). Simulations resulting from different evapotranspiration modules are displayed in blue ( $ET_{ASCE}$ ), yellow ( $ET_{FAO}$ ), and green ( $ET_{Haude}$ ), the solid (SPASS) and dashed (CERES) lines stand for the chosen plant module.

On rainy days, when maximum temperature and radiation were low, modeled sap flow rates were lower than on the other days and yielded between 20 and 100 mm h<sup>-1</sup>. During most nights, no sap flow was modeled by any of the six model configuration. Only when ET<sub>ASCE</sub> was applied in combination with SPASS, sap flow rates of up to 5 mm h<sup>-1</sup> at 12 nights during the period of interest were simulated.

The diurnal cycles and the differences among the models can be more clearly seen in Fig. 3, which shows averaged diurnal cycles of modeled and measured transpiration between 14 Aug. (DOY 226) and 9 Sept. (DOY 252) 2013. Figure 3a shows the averaged lysimeter transpiration over all days. The daily maximum of measured transpiration is 0.060 mm h<sup>-1</sup>, the CERES simulations showed daily maxima of about 0.069 mm h<sup>-1</sup>, and the SPASS simulations peak around 0.052 mm h<sup>-1</sup>. On average, the influence of the plant model on the transpiration is higher than the influence of the ET module. This is also valid when only the non-rainy days are considered (Fig. 3c), but then the daily maximum of transpiration is between 0.004 and 0.008 mm h<sup>-1</sup> higher in comparison to Fig. 3a. On rainy days (Fig. 3b), transpiration peaks at 0.019 mm h<sup>-1</sup> and has a low daily amplitude. Here, the influence of the ET module on the model behavior is more distinct. The ET<sub>FAO</sub> simulations exhibit maximum values of 0.033 (SPASS) and 0.042 (CERES) mm h<sup>-1</sup>, the ET<sub>ASCE</sub> simulations have maxima between 0.017 (SPASS) and 0.025 (CERES) mm h<sup>-1</sup>, and the ET<sub>Haude</sub> simulations peak at 0.014 (SPASS) and 0.019 (CERES) mm h<sup>-1</sup>.

In general, all six simulations are in agreement with the measurements. However, simulated sap flow was higher than measured on most of the rainy days and lower during night. From 3 Sept. (DOY 246) 2013, all simulations underestimate the measurements,

SPASS simulations more evidently than CERES simulations. In Table 4, indices of agreement (IA) and Nash–Sutcliffe model efficiency coefficients (NSE) between simulated and measured sap flow are shown. In total, 624 points in time (hourly values on 26 d) were compared. The IAs are very similar for all model runs and range between 0.90 and 0.94. There is a tendency of ET<sub>FAO</sub> performing slightly worse than the other two ET models. In the case of SPASS application, ET<sub>ASCE</sub> and ET<sub>Haude</sub> perform similarly, while in the case of CERES applications, ET<sub>ASCE</sub> facilitates better results when the NSE is considered.

One reason for the slightly different performance of the ET<sub>ASCE</sub> and the SPASS approach is the time resolution. Since ET<sub>pot</sub> and  $T_{pot}/T_{act}$  are newly calculated in every time step the model can quickly react to changes in the input weather data, such as radiation or relative humidity. Even at night time the modeled potential and actual transpiration can be higher than zero, when ET<sub>ASCE</sub> and SPASS are combined, which is in accordance with our measurements. The distribution of ET<sub>pot</sub> and  $T_{pot}/T_{act}$  over the day that is used by ET<sub>FAO</sub>, ET<sub>Haude</sub>, and CERES is reasonable in summer time, thus during our measurement period, but daytime might be assumed too long from autumn to spring. All these approaches set nighttime potential evapotranspiration to zero. Especially at the beginning and at the end of each day, sap flow rates were quickly increasing and decreasing. At this point in time the largest errors occurred because the same measured and modeled values arose with a small time lag. Here, the ET<sub>ASCE</sub> approach takes minor advantage of the non-fixed ET distribution over the day in comparison to the other two approaches.

On rainy days, all simulations overestimated the measured sap flow. The plants did not transpire much due to the high relative

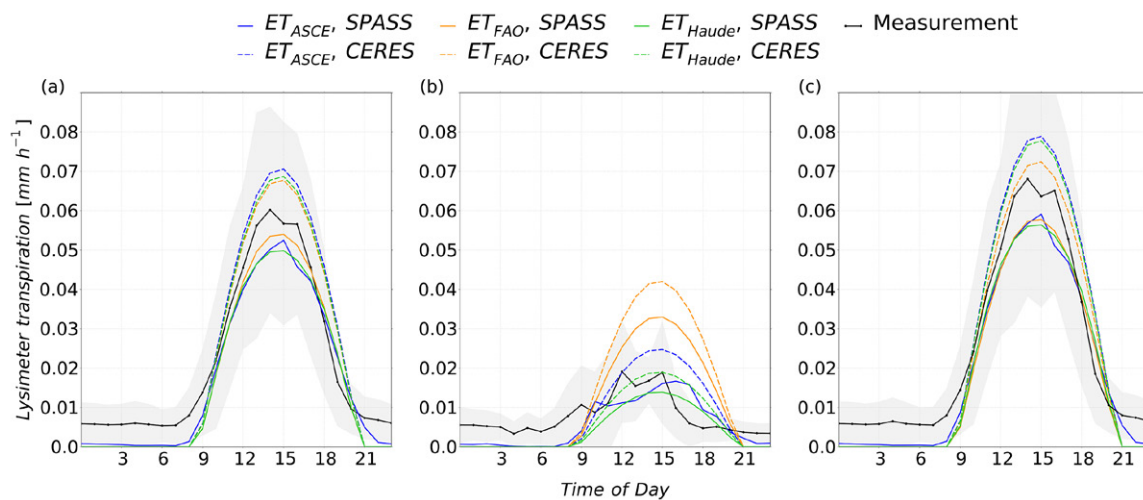


Fig. 3. Averaged diurnal cycles of measured and simulated lysimeter transpiration between 14 Aug. and 9 Sept. 2013: (a) all days, (b) rain days (19, 25, 27 Aug. and 8 Sept. 2013), (c) non-rain days. The measured values (solid black line with dots) are hourly averaged sums of transpiration [mm h<sup>-1</sup>] from five different maize plants on one lysimeter and comprise standard deviations (gray shaded). Simulations resulting from different evapotranspiration modules are displayed in blue (ET<sub>ASCE</sub>), yellow (ET<sub>FAO</sub>) and green (ET<sub>Haude</sub>), the solid (SPASS) and dashed (CERES) lines stand for the chosen plant module.

Table 4. Indices of agreement (IA) and Nash–Sutcliffe model efficiency coefficients (NSE) between measured and simulated sap flow between 14 Aug. and 9 Sept. 2013 (624 pairs of variates).

| Configuration                   | IA    |       | NSE   |       |
|---------------------------------|-------|-------|-------|-------|
|                                 | SPASS | CERES | SPASS | CERES |
| ET <sub>ASCE</sub> <sup>†</sup> | 0.92  | 0.94  | 0.71  | 0.71  |
| ET <sub>FAO</sub>               | 0.90  | 0.92  | 0.65  | 0.69  |
| ET <sub>Haude</sub>             | 0.92  | 0.94  | 0.71  | 0.69  |

† ET is evapotranspiration.

humidity and the low solar radiation. However, all models still show  $T_{act}$  significantly larger than zero. Since soil water does not limit transpiration on these days,  $T_{pot}$  and  $T_{act}$  are the same.  $T_{pot}$  in turn, mainly depends on  $ET_{pot}$ , which might be larger than it should be. The numerator in the equations of  $ET_{ASCE}$  and  $ET_{FAO}$  approach consists of two summands. The first depends on the radiation and the second on relative humidity. When relative humidity is high, the second summand approaches zero, while the first one can still be significantly larger than zero. The application of daily averaged weather data ( $ET_{FAO}$ ) seems to be a disadvantage on those days. In the  $ET_{Haude}$  case,  $ET_{pot}$  only depends on temperature and relative humidity, which is beneficial on the rainy days. Another issue that could lead to this overestimation by the models during the rainy days is that none of the ET models directly considers leaf stomatal conductance. Thus, the regulation of stomatal opening due to actual radiation (Rochette et al., 1991) was not simulated and led therefore to the respective overestimation. Furthermore, our models did not include rainfall interception. In contrast to the sap flow simulations we observed water interception by the leaves which fulfilled the evaporative demand from the atmosphere. Once the interception water had evaporated, transpiration could start to recover.

From 15 to 18 Aug. (DOYs 227–230) 2013 in case of SPASS application, simulations of  $T_{pot}$  are partly higher than the simulations

of  $T_{act}$  and higher than the measured sap flow. In these periods, the simulated LAI (Fig. 4) is near its maximum and thus leads to the distribution of a large fraction of  $ET_{pot}$  to  $T_{pot}$ . However, soil water contents in the rooted soil layers, which limit transpiration, decline from the first to the fourth day. This decreases simulated  $T_{act}$ , which overestimates the measured sap flow at the beginning of this period, but slightly underestimates it at the end. However, in the case of CERES application, little to no water stress occurred. This is mainly due to higher simulated root length densities in comparison to the SPASS model. From 24 Aug. (DOY 236) 2013 to the end of the analyzed period,  $T_{pot}$  and  $T_{act}$  are equal and only show minor differences from the sap flow measurements. The underestimation at the very end is due to a slightly too fast decline of modeled LAI (Fig. 4). During the period of sap flow measurements, the SPASS simulations generally have lower LAI values than the CERES simulations. As a consequence, sap flow is larger in the CERES simulations. The importance of the correct representation of the LAI was also shown by van Griensven et al. (2014), who found that accurate LAI values improved evapotranspiration simulations over forest regions. Since both applied models of our study originally are canopy models, pot effects in the lysimeter and boundary effects on the lysimeter wall might have occurred in reality, but were not represented in the models. These effects among others could be given by hampered sideward root growth at the lysimeter walls and increased downward root growth to the bottom, where water concentrates at the outflow boundary of the lysimeter. For instance, Berliner and Oosterhuis (1987) identified increased root length densities of wheat plants below 0.6 m in lysimeters, while in the control field root length density was monotonously decreasing with soil depth. In their study, the plants on the lysimeters experienced water stress later than those in the field, but stressed conditions also occurred more abruptly. Manoli et al. (2015) performed a modeling study on spatially distributed crop yields and found that the root depth has a strong influence on maize yield and transpiration simulations. However, in our study, an increase of maximum rooting depth from 80 to 200 cm did not influence the simulations since there was enough water in the top

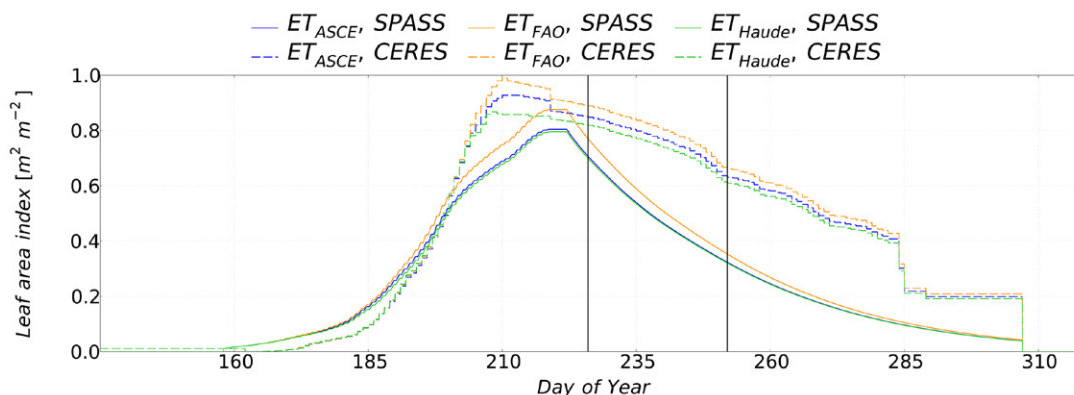


Fig. 4. Time series of simulated leaf area indices (LAIs) from 15 May to 15 Nov. 2013. Simulations resulting from different evapotranspiration modules are displayed in blue ( $ET_{ASCE}$ ), yellow ( $ET_{FAO}$ ) and green ( $ET_{Haude}$ ), the solid (SPASS) and dashed (CERES) lines stand for the chosen plant module. The vertical solid black lines show the period of the sap flow measurements from 14 Aug. to 9 Sept. 2013.

soil layers during the root growth phases, which hampered further root depth growth when the roots reached the 80-cm soil depth.

## Simulations of Leaf Area Index

In Fig. 4, LAI simulations by the different models from 15 May (DOY 135) to 15 Nov. (DOY 319) 2013 are shown. The crop model drives the leaf area development while there is a small influence of the respective ET model. After emergence, the LAI simulated by the SPASS model is rapidly increasing and reaches maximum values of about  $0.8 \text{ m}^2 \text{ m}^{-2}$  ( $ET_{ASCE}$  and  $ET_{HauDe}$ ), and  $0.88 \text{ m}^2 \text{ m}^{-2}$  ( $ET_{FAO}$ ) at 9 Aug. (DOY 221) 2013, which marks the end of the vegetative phase. In the subsequent, generative phase, the LAI is smoothly decreasing due to leaf senescence depending on the developmental age. The model also takes senescence due to shading ( $LAI > 4 \text{ m}^2 \text{ m}^{-2}$ ) into consideration, which was not the case in this study. From 14 Aug. (DOY 226) to 9 Sept. (DOY 252) 2013, the simulated LAI is declining from approximately  $0.75$  to  $0.35 \text{ m}^2 \text{ m}^{-2}$ . At the beginning and at the end of the growth period (until DOY 180 and from DOY 280), there is very little influence of the chosen evapotranspiration module on the model results. In the CERES model, the LAI is slowly increasing after emergence and peaks around 29 July (DOY 210):  $0.93 \text{ m}^2 \text{ m}^{-2}$  ( $ET_{ASCE}$ ),  $0.99 \text{ m}^2 \text{ m}^{-2}$  ( $ET_{FAO}$ ), and  $0.87 \text{ m}^2 \text{ m}^{-2}$  ( $ET_{HauDe}$ ). In the following phase, the LAI first decreases very slowly and then faster. From 10 Oct. (DOY 283) 2013, stepwise drops of LAI are simulated. From 22 July (DOY 203), the choice of the evapotranspiration module becomes evident in the LAI simulations. During the period of sap flow measurements, the LAI decreases by about 30%. Leaf area growth occurs until CERES development stage 3, which ends on 30 July (DOY 211). Leaf senescence, which is closely related to development stages, already takes place from CERES development stage 2, but becomes more evident when the leaf growth stops. The stepwise decrease of LAI is caused by different representations of leaf senescence at different CERES development stages. One might be surprised by the quite low values of simulated LAI. However, the plant density of  $5 \text{ plants m}^{-2}$  on the lysimeter was lower than on a standard field where plant densities range between 6 and 10 plants  $\text{m}^{-2}$  depending on the variety and the water supply. To calculate the LAI, the plant density is directly multiplied with the calculated leaf area per plant. In addition, 2013 was a poor maize year in Germany, especially in Bavaria, where yields of grain and silage maize were about 20% lower than the long term average due to unfavorable climate conditions, i.e., long drought periods. Moreover, the very sandy soils in the lysimeter have increased water and nutrient stress due to the low soil water capacity and nutrient storage, which is also represented in the model.

The LAI simulations generally depend on the simulation of phenological development (not shown). All plants on the lysimeter emerged until the beginning of June, but did not reach maturity ( $BBCH < 90$ ). Since the simulated phenological development stages only depend on temperature sums, the choice of the evapotranspiration module does not influence the model results.

However, the phenological development is influenced by the choice of the plant model. SPASS only distinguishes between temperature sums during the vegetative and the generative phase. As a result the development curve is very smooth and continuous. Emergence is simulated at the beginning of June 2013. The CERES model has nine different development phases, which leads, compared to the SPASS development, to the simulation of faster phenological development in some periods and slower development in other periods. Emergence occurred at the end of May 2013. Because of this earlier emergence the phenological development of the CERES model in this study is always ahead of the SPASS model. Therefore, within the simulation period, the CERES model reaches the final BBCH stage of 92, but the SPASS model finishes at 80.

## Measurements and Simulations of Soil Water Contents

Measured and modeled soil water contents at the 10-, 50- and 80-cm depths are displayed in Fig. 5. In the 50-cm depth, measured soil water contents were in the range between  $0.15$  and  $0.34 \text{ cm}^3 \text{ cm}^{-3}$  and in the 80-cm depth were between  $0.15$  and  $0.24 \text{ cm}^3 \text{ cm}^{-3}$ . Short-term variability was also higher in the upper soil layer. In both depths, the maximum soil water contents were measured at 1 June (DOY 152), while in the 50-cm depth the minimum soil water content was registered at 24 Aug. (DOY 236) 2013 and in the 80-cm depth at 10 Sept. (DOY 253) 2013. The simulated soil water contents lie between  $0.23$  and  $0.38 \text{ cm}^3 \text{ cm}^{-3}$  in the 10-cm depth, between  $0.2$  and  $0.33 \text{ cm}^3 \text{ cm}^{-3}$  in the 50-cm depth, and between  $0.17$  and  $0.25 \text{ cm}^3 \text{ cm}^{-3}$  in the 80-cm depth. The simulated soil water contents in 10-cm depth show the largest variabilities. The 50- and 80-cm depth soil water contents have their extremes at the same points in time as the measured values.

Until the beginning of March (around DOY 60), the soil water content simulations of the different model configurations do not differ significantly due to the absence of plants and low temperature and radiation leading to very similar  $ET_{pot}$  (and thus  $ET_{act}$ ) simulations. From then, in the three depths, the highest soil water contents are simulated by the use of  $ET_{HauDe}$  approach, the lowest in case of  $ET_{FAO}$ . At zero LAI,  $ET_{pot}$  is completely partitioned to  $E_{pot}$  and thus to  $E_{act}$  (Eq. [5]). When temperature and radiation increase, differences of  $ET_{pot}$  simulations among the three evapotranspiration modules become more evident. As a consequence, a different amount of water is removed from the top soil, which then propagates to lower soil layers. At the beginning of June (around DOY 152), there was again high water input due to precipitation leading to an equalization of all models and to the highest simulated water contents in 2013. When plant emergence occurred at the end of May (SPASS) and beginning of June (CERES), differences resulting from plant submodule choice evolved in the dynamics of the modeled soil water contents. These differences between the simulations become more evident when the water contents get lower, while they assimilate when there was water input. These divergences get larger from 20 July (DOY 201)

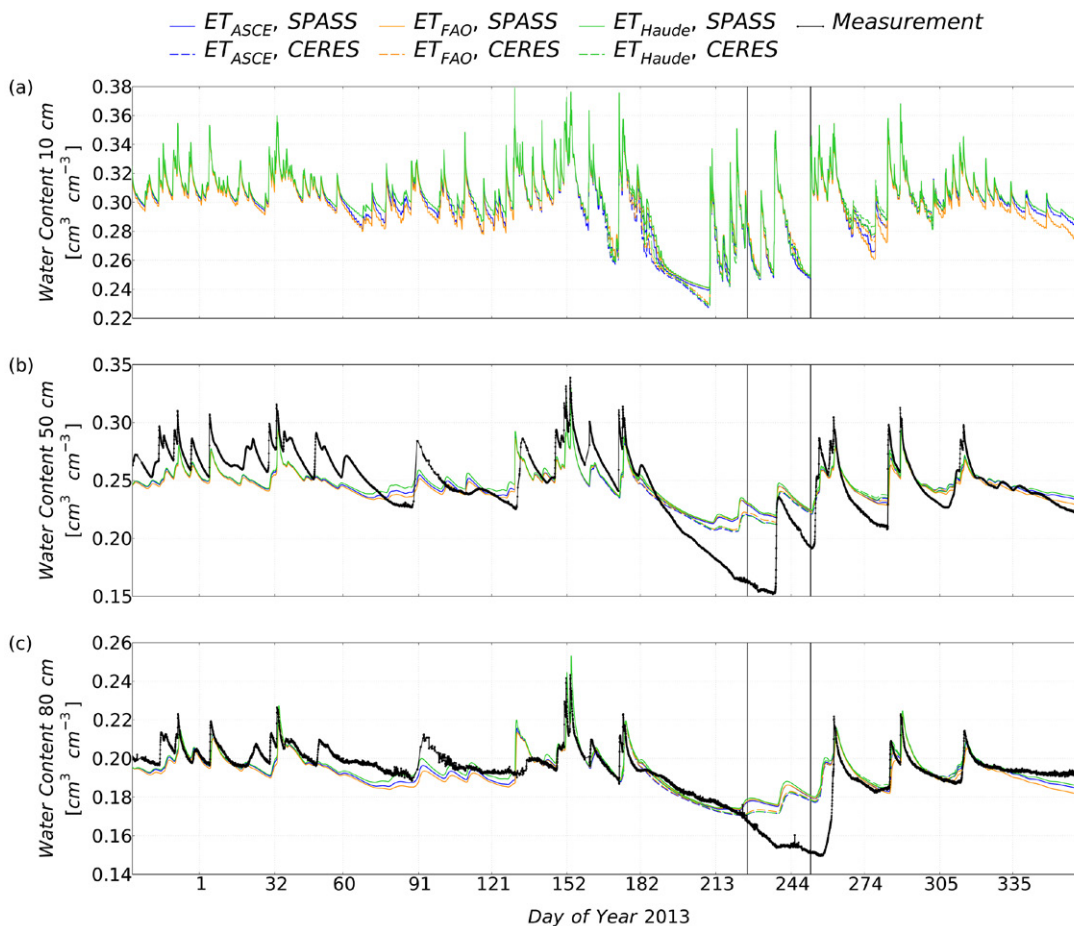


Fig. 5. Time series of measured (solid black line with dots) and simulated soil water contents [ $\text{cm}^3 \text{cm}^{-3}$ ] in the (a) 10-cm, (b) 50-cm, and (c) 80-cm depths from 4 Dec. 2012 to 31 Dec. 2013. The  $x$  axis grid lines are placed at the first day of each month. Simulations resulting from different evapotranspiration modules are displayed in blue ( $ET_{ASCE}$ ), yellow ( $ET_{FAO}$ ) and green ( $ET_{Haude}$ ), the solid (SPASS) and dashed (CERES) lines stand for the chosen plant module. The vertical solid black lines show the period of the sap flow measurements from 14 Aug. to 9 Sept. 2013.

in the 10- and 50-cm depths, and about 10 d later in the 80-cm depths. In all depths, the  $ET_{ASCE}$  and  $ET_{Haude}$  water contents are higher than those of  $ET_{FAO}$  when SPASS is applied. The CERES simulations show the highest water contents in combination with  $ET_{FAO}$  in the three depths. Comparing simulations that apply the same evapotranspiration module, but a different plant module, the soil water contents of the CERES simulations are lower until 1 September (DOY 244) (up to  $0.01 \text{ cm}^3 \text{ cm}^{-3}$  in the 10- and 50-cm depths and  $0.007 \text{ cm}^3 \text{ cm}^{-3}$  in the 80-cm depth) than those of the corresponding SPASS simulations.

The explanation is differently simulated LAIs: From 19 July (DOY 200) the LAI (Fig. 4) simulated by SPASS is lower than in the CERES model simulations, which means that more evaporation and less transpiration occur. Hence, more water is depleted from the top soil layer, while there remains a significant amount of water to flow downward. In the CERES model, the LAI remains higher which allows the model to partition a larger fraction of  $ET_{pot}$  to  $T_{pot}$ . As a consequence, water is still taken up from the rooted soil layers, and thus, reduces soil water contents throughout the whole

soil profile. Another reason for the lower soil water contents of the CERES simulations in comparison to SPASS is the higher root length density, which allows the CERES model to deplete more water from each layer.

In the 50- and 80-cm soil depths, the water content simulations are in good agreement with the measurements. The measured peaks are simulated by the models, but especially when water contents drop below  $0.23 \text{ cm}^3 \text{ cm}^{-3}$  in the 50-cm depth and below  $0.17 \text{ cm}^3 \text{ cm}^{-3}$  in the 80-cm depth, there are some differences between measurements and simulations. The IA and NSE values of the different model configurations are shown in Table 5. Since there are long periods (in total about 8 mo) where simulated water contents only differ slightly among the model configurations, the statistical measures are very similar at both measurement depths. The dynamics of the soil water contents in the 50-cm depth (IA between 0.77 and 0.83, NSE between 0.55 and 0.63) are as well represented by the models as the dynamics of the soil water contents in the 80-cm depth (IA between 0.80 and 0.85, NSE between 0.49 and 0.60). There is a minor tendency of  $ET_{Haude}$ , CERES performing better

Table 5. Indices of agreement (IA) and Nash–Sutcliffe model efficiency coefficients (NSE) between measured and simulated soil water content at the 50- and 80-cm depths. Columns denote the two applied plant submodules, the rows the different evapotranspiration submodules. All available pairs of variates (5796) between 4 Dec. 2012 and 31 Dec. 2013 are compared.

| Configuration        | IA                       |       |                          |       | NSE                      |       |                          |       |
|----------------------|--------------------------|-------|--------------------------|-------|--------------------------|-------|--------------------------|-------|
|                      | Soil water content 50 cm |       | Soil water content 80 cm |       | Soil water content 50 cm |       | Soil water content 80 cm |       |
| Configuration        | SPASS                    | CERES | SPASS                    | CERES | SPASS                    | CERES | SPASS                    | CERES |
| ET <sub>ASCE</sub> † | 0.78                     | 0.82  | 0.82                     | 0.85  | 0.57                     | 0.63  | 0.53                     | 0.59  |
| ET <sub>FAO</sub>    | 0.77                     | 0.81  | 0.80                     | 0.83  | 0.55                     | 0.60  | 0.49                     | 0.54  |
| ET <sub>Haude</sub>  | 0.77                     | 0.83  | 0.81                     | 0.85  | 0.55                     | 0.63  | 0.52                     | 0.60  |

† ET is evapotranspiration.

than the other five model configurations. These NSE values are higher than those achieved by Stumpp et al. (2012), who evaluated soil water contents in five lysimeters. Depending on the soil depth, they found NSEs between  $-9.51$  and  $0.05$  for the least accurately simulated lysimeter and NSEs between  $-0.4$  and  $0.46$  in the most accurately simulated lysimeters. Herbst et al. (2005) evaluated different soil water flow models and found IAs higher than  $0.9$  in the 25- and 85-cm soil depths when a one-dimensional Richards equation model was applied while the capacity based model performed not as good.

In our simulations, there are several reasons for deviations between models and measurements. In some periods, simulated  $ET_{act}$  was too high, which can be a result of intense evaporation from the top soil layer and/or of strong plant water uptake from the rooted soil layers. The latter is in agreement with the overestimation of sap flow or transpiration by the models on rainy days characterized by low daily maxima of sap flow rates (Fig. 2 and 3). While the measurements of soil water contents suggest that the water in the soil was absorbed by the plants in deeper soil layers, in the simulations soil water was already depleted in the upper soil layers. This can be seen in Fig. 4 where the simulated 10-cm water content strongly drops from  $0.3 \text{ cm}^3 \text{ cm}^{-3}$  to  $0.23$  (CERES)/ $0.24$  (SPASS)  $\text{cm}^3 \text{ cm}^{-3}$  during July, while the models start to overestimate the measurements in the 50-cm depth. In the following period until the end of the sap flow measurements, this overestimation becomes also evident in 80-cm depth, while in the simulations the rain water is depleted in the 10-cm depth immediately after water input. Some uncertainty might result from uncertainty in the model parameters, such as soil hydraulic conductivity (Mishra and Parker 1989). This parameter is difficult to estimate in natural soils due to local heterogeneities of porosity and due to soil aggregation over time. Therefore, different soil hydraulic conductivities were tested, but our model results could not be improved.

## Water Balance

Daily sums of measured and simulated evapotranspiration, percolation, and water content change of the whole soil column are shown in Fig. 6. The measured ET was strongly changing from day to day, so that in the beginning of August a day with no ET was followed

by the day with the maximum registered daily ET of  $3.8 \text{ mm d}^{-1}$ . Already in May daily ET of up to  $2.5 \text{ mm d}^{-1}$  was observed. From the beginning of October maximum daily ET was around  $1.0 \text{ mm d}^{-1}$ . Daily percolation was mostly lower than  $2 \text{ mm d}^{-1}$ , but five distinct peaks between  $4$  and  $22 \text{ mm d}^{-1}$  were registered. The daily soil water content change was in the range between  $-35$  and  $38 \text{ mm d}^{-1}$ . These extreme values were observed between the end of May and beginning of June. A negative soil water content change can be related to either percolation or evapotranspiration. Large negative values mostly occur during the percolation peaks (if there is no additional water input), while the loss of soil water is lower when only evapotranspiration occurs.

The simulated daily ET rates were also rapidly changing from day to day. The highest simulated ET was  $4.7 \text{ mm d}^{-1}$ . However, there are two longer periods where modeled ET was constantly around  $1 \text{ mm d}^{-1}$ : mid July (DOY 192–210) and the beginning of September (DOY 244–250). Both periods were characterized by longer absence of rain leading to very low water contents in the top soil layer and thus to a limitation of evaporation. Partly, transpiration was also limited during these periods, but not as much as evaporation due to water depletion from deeper soil layers. Especially until 6 Aug. (DOY 218) 2013, the CERES simulations show higher evapotranspiration than the SPASS model runs. Simulated percolation is mostly lower than  $2 \text{ mm d}^{-1}$ , but six peaks were simulated, five of those between  $3$  and  $10 \text{ mm d}^{-1}$ , and one larger peak with  $40 \text{ mm d}^{-1}$ . Daily soil water content change was simulated in the range between  $-38$  and  $40 \text{ mm d}^{-1}$ .

While measured percolation and soil water content change are well simulated by the models, they lack to a certain extent the correct simulation of evapotranspiration. The IAs and NSEs of the different model configurations are shown in Table 6. Considering these two statistical means, percolation and soil water content change are best simulated when  $ET_{Haude}$  was applied, although the IA shows less variation than the NSE. When simulated and measured ET rates are compared, the NSEs are around zero or slightly below, which means that the average of the measurements is as good as the simulation. Applying the NSE, the  $ET_{FAO}$ , SPASS simulations perform best, but considering the IA, the  $ET_{Haude}$ ,

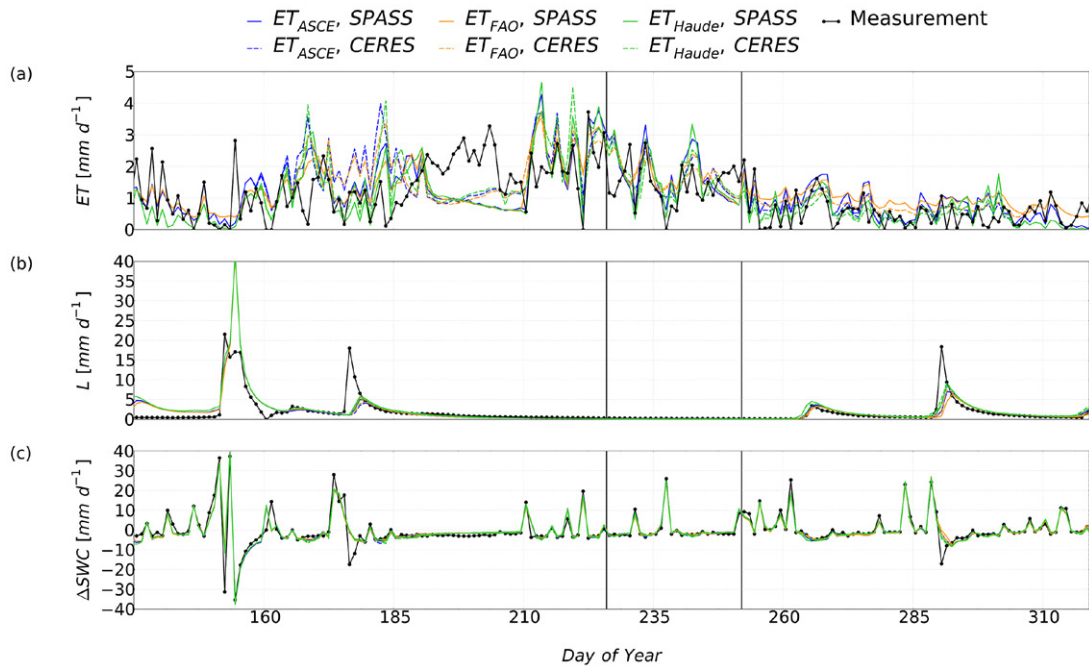


Fig. 6. Time series of the measured (solid black line with dots) and the simulated daily lysimeter water balance from 15 May to 15 Nov. 2013: (a) actual evapotranspiration, (b) percolation, and (c) water content changes of the whole soil column. Simulations resulting from different evapotranspiration modules are displayed in blue ( $ET_{ASCE}$ ), yellow ( $ET_{FAO}$ ), and green ( $ET_{Haude}$ ), the solid (SPASS) and dashed (CERES) lines stand for the chosen plant module. The vertical solid black lines show the period of the sap flow measurements from 14 Aug. to 9 Sept. 2013.

Table 6. Indices of agreement (IA) and Nash–Sutcliffe model efficiency coefficients (NSE) between measured and simulated evapotranspiration, percolation and soil water content change. Columns denote the two applied plant submodules, the rows the different evapotranspiration submodules. The total number of pair of variates is 184 representing daily values between 15 May and 15 Nov. 2013.

| Variable†    | Configuration | IA    |       | NSE   |       |
|--------------|---------------|-------|-------|-------|-------|
|              |               | SPASS | CERES | SPASS | CERES |
| ET           | $ET_{ASCE}$   | 0.71  | 0.68  | -0.01 | -0.10 |
|              | $ET_{FAO}$    | 0.66  | 0.65  | 0.04  | -0.04 |
|              | $ET_{Haude}$  | 0.73  | 0.71  | -0.01 | -0.08 |
| P            | $ET_{ASCE}$   | 0.83  | 0.83  | 0.30  | 0.32  |
|              | $ET_{FAO}$    | 0.82  | 0.83  | 0.30  | 0.31  |
|              | $ET_{Haude}$  | 0.84  | 0.85  | 0.33  | 0.34  |
| $\Delta SWC$ | $ET_{ASCE}$   | 0.96  | 0.96  | 0.85  | 0.85  |
|              | $ET_{FAO}$    | 0.95  | 0.96  | 0.84  | 0.85  |
|              | $ET_{Haude}$  | 0.96  | 0.96  | 0.86  | 0.86  |

† ET, evapotranspiration; P, precipitation;  $\Delta SWC$ , water content change of the whole soil column.

SPASS performs better. In general, the SPASS simulations show marginally higher IAs and NSEs than the corresponding CERES simulations. Total, summed up measured ET from 15 May to 15 Nov. 2013 was 198.0 mm.  $ET_{Haude}$  combined with SPASS and CERES underestimate this sum by only 1.4 and 3.3%. The other simulations show a minor overestimation by 12.2% ( $ET_{ASCE}$ , SPASS) to 17.2% ( $ET_{FAO}$ , SPASS). The measured cumulative

percolation from 15 May to 15 Nov. 2013 amounted to 325.0 mm, while the simulations showed values between 346 mm (both  $ET_{FAO}$  simulations) and 385 mm ( $ET_{Haude}$ , SPASS). The overestimation of cumulative drainage by our models is contradictory to Skaggs et al. (2006b), who found during a 2-wk period that the HYDRUS model slightly underestimated measured percolation. However, they applied a seepage face boundary condition where drainage only occurs when the bottom soil layer is saturated (Šimůnek et al., 1998), while we achieved the best results assuming free drainage. This boundary condition was also successfully applied by Loos et al. (2007) to the same lysimeters. However, the stratification with gravel at the bottom of the lysimeter (increasing size of gravel with increasing depth) might represent a boundary condition that is somehow “between” the seepage and the free drainage approach. The measured total change of soil water contents was a gain of 8.7 mm throughout the presented period, while all the models simulated a minor loss of about 10 mm.

Linking together statistics with cumulative ET suggests that there are some periods where ET was overestimated by the models and other periods where it was underestimated. This can also be observed in Fig. 6a: From DOYs 159 to 187 and from 212 to 245 simulated ET is mostly higher than the measured ET, while from DOYs 191 to 209 and from 245 to 252 simulated ET is lower than the measurements. The overestimation of ET mainly occurs during periods with high precipitation. In these periods, simulated actual transpiration was not limited since water was available in the rooted soil layers, especially in the upper soil, leading to an overestimation

by the models (see days with precipitation and after rain events of Fig. 2). Likewise, potential evaporation was not limited by soil water availability in the first soil layer. As a consequence, in the models water is depleted from the top soil layer, whereas in reality it was later available for plant uptake in deeper soil layers or even percolated. Corresponding to this fact, from DOYs 160 to 190 the simulated water contents in the 50-cm depth were up to  $0.03 \text{ cm}^3 \text{ cm}^{-3}$  lower than measured (Fig. 5), and the percolation peak at 25 June (DOY 176) was likewise underestimated by the models and was simulated 2 d later than measured. In the following period, there was very little water input to the system, leading to limitations of simulated evaporation and transpiration, but the measurements suggest stronger water uptake from deeper soil layers.

As precipitation did not occur during 3 wk in July, the plants might have been water-stressed, which could have had an impact on root growth. The root length distribution, which in the models exponentially decreases from the top to bottom soil layers, might not reflect reality. Huck et al. (1983) investigated water stress adaptations of soybeans in a sandy soil by comparing a natural rainfall treatment and a treatment with additional irrigation. In the irrigated system root growth was decreasing with soil depth, but in the water-stressed system root growth was generally higher. Maximum root growth was observed in the 120-cm depth, while top soil roots got senescent. Sharp and Davies (1985) investigated drought effects on water uptake and root growth of maize plants. In drier soils, root growth in the upper soil layers was restricted, while more intense root growth was observed below the 60-cm depth. Additionally, the deeper roots of the water-stressed plants showed higher water uptake rates per unit root length density than the roots in the upper soil layers. Carminati et al. (2009) explained this phenomenon by contact loss between roots and soil due to root shrinkage during dryer periods. They found that after rewet events, some of the roots grew again and regained contact to the soil, but especially around older taproots the gaps remained. However, in a follow-up publication, Carminati et al. (2013) identified that a decrease of transpiration and soil matric potential was the trigger for the contact loss of roots. They describe a conceptual model in which the process of gap formation is self-enhancing because of the reduced hydraulic conductivity between root and soil.

## Summary and Conclusions

Sap flow and evapotranspiration of maize plants on a weighing lysimeter were measured and analyzed in the summer of 2013. The water balance of the lysimeter system and other processes, which occur in the soil–plant system, were simulated with the modular model framework Expert-N. Six different model configurations with varying evapotranspiration and plant submodules were applied.

We successfully applied sap flow measurement devices using the HRM to measure water transport in maize plants on lysimeters.

In general, the simulations of transpiration agreed with the sap flow measurements. The daily transpiration determined by sap flow measurements was lower than the daily lysimeter evapotranspiration and of the same order of magnitude. In the future, these devices can also be applied to measure transpiration of maize during scientific field studies or to determine the plant water demand in the field to ensure demand-based irrigation. The devices, which were used in this study, are easy to install, but a constant power supply must be guaranteed to run them permanently.

Some model configurations better represented the measurements than others. All model configurations were able to well simulate the hourly sap flow measurements during daytime, but lacked the representation of measured nighttime transpiration. The use of the  $ET_{ASCE}$  evapotranspiration module, which accounts for hourly weather changes, is beneficial when high-resolution transpiration is to be simulated.

Lysimeters are a very powerful means to evaluate water balance simulations. All model configurations satisfyingly simulated measured daily percolation and soil water contents, but lacked the representation of daily evapotranspiration. When considering the seasonal water balance, surprisingly the very simple Haude approach seems to provide a suitable value for potential evapotranspiration, which allows for the calculation of actual transpiration and evapotranspiration. However, one must notice that this approach was developed to match evapotranspiration in the region of our study. Nevertheless, on rainy and moist days the lack of a radiation term in the Haude approach might be beneficial in comparison to the Penman–Monteith approaches, which more strongly overestimate evapotranspiration on those days. In principle, all model configurations can be applied for future simulations, but one should always consider the specific research question to generate a suitable model configuration.

An important issue, which may lead to deficiencies in the simulations, is the distribution of water within the soil profile. During rewetting events after drought periods, simulated evapotranspiration is higher than measured while during the following drier periods the soil available water is missing for plant uptake. Key parameters that are responsible for the strongest differences among the different transpiration simulations are root length densities and the LAI, which determine water uptake from the soil and the distribution of potential evapotranspiration into the plant and the soil part.

## Acknowledgments

This work was supported by the German Research Foundation (DFG) in the framework of the Research Unit FOR 1695 “Agricultural Landscapes under Global Climate Change—Processes and Feedbacks on a Regional Scale.” We also gratefully acknowledge the support by the TERENO (Terrestrial Environmental Observatories) funded by the Helmholtz-Gemeinschaft. Christian Biernath was funded by the Helmholtz project “REKLIM—Regional Climate Change.” Christian Klein was funded by the HGF Alliance “Remote Sensing and Earth System Dynamics” (EDA). Special thanks go to Heinz Lösslein from the Meteorological Institute Munich, who provided the weather data, and to the Helmholtz Research School MICMoR, which supports my scientific and professional development.

# References

- Allen, R.G., L.S. Pereira, D. Raes, and M. Smith. 1998. Crop evapotranspiration: Guidelines for computing crop water requirements. FAO, Rome.
- Becker, P., and W.R.N. Edwards. 1999. Corrected heat capacity of wood for sap flow calculations. *Tree Physiol.* 19(11):767–768. doi:10.1093/treephys/19.11.767
- Beniston, M., D.B. Stephenson, O.B. Christensen, C.A.T. Ferro, C. Frei, S. Goyette, K. Hasnaes, T. Holt, K. Jylhä, B. Koffi, J. Palutikof, R. Schöll, T. Semmler, and K. Woth. 2007. Future extreme events in European climate: An exploration of regional climate model projections. *Clim. Change* 81:71–95. doi:10.1007/s10584-006-9226-z
- Berliner, P.R., and D.M. Oosterhuis. 1987. Effect of root and water distribution in lysimeters and in the field on the onset of crop water stress. *Irrig. Sci.* 8:245–255. doi:10.1007/BF00257509
- Biernath, C., S. Gayler, S. Bittner, C. Klein, P. Högy, A. Fangmeier, and E. Priesack. 2011. Evaluating the ability of four crop models to predict different environmental impacts on spring wheat grown in open-top chambers. *Eur. J. Agron.* 35(2):71–82. doi:10.1016/j.eja.2011.04.001
- Brisson, N., B. Itier, J.C. L'Hotel, and J.Y. Lorendeau. 1998. Parameterisation of the Shuttleworth–Wallace model to estimate daily maximum transpiration for use in crop models. *Ecol. Model.* 107:159–169. doi:10.1016/S0304-3800(97)00215-9
- Buckley, T.N., T.L. Turnbull, S. Pfautsch, and M.A. Adams. 2011. Nocturnal water loss in mature subalpine *Eucalyptus delegatensis* tall open forests and adjacent *E. pauciflora* woodlands. *Ecol. Evol.* 1(3):435–450. doi:10.1002/ece3.44
- Burgess, S.S.O., M.A. Adams, N.C. Turner, C.R. Beverly, C.K. Ong, A.A.H. Khan, and T.M. Bleby. 2001. An improved heat pulse method to measure low and reverse rates of sap flow in woody plants. *Tree Physiol.* 21(9):589–598. doi:10.1093/treephys/21.9.589
- Campbell, G.S. 1986. Soil physics with BASIC, transport models for soil plant systems. *Developments in Soil Science* 14. Elsevier, New York.
- Carminati, A., D. Vetterlein, N. Koebernick, S. Blaser, U. Weller, and H.-J. Vogel. 2013. Do roots mind the gap? *Plant Soil* 367:651–661. doi:10.1007/s11104-012-1496-9
- Carminati, A., D. Vetterlein, U. Weller, H.-J. Vogel, and E. Oswald Sascha. 2009. When roots lose contact. *Vadose Zone J.* 8:805–809. doi:10.2136/vzj2008.0147
- Childs, S.W., and R.J. Hanks. 1975. Model of soil salinity effects on crop growth. *Soil Sci. Soc. Am. J.* 39:617–622. doi:10.2136/sssaj1975.03615995003900040016x
- Christensen, J.H., and O.B. Christensen. 2003. Climate modelling: Severe summertime flooding in Europe. *Nature* 421:805–806. doi:10.1038/421805a
- de Vries D.A. 1952. The thermal conductivity of soil. *Mededelingen van Lanbouwhogeschool, Wageningen, the Netherlands.*
- de Vries, D.A. 1963. Thermal properties of soils In: W. Van Wijk, editor, *Physics of plant environment.* North-Holland Publishing Co., Amsterdam. p. 210–235.
- Ding, R., S. Kang, Y. Zhang, X. Hao, L. Tong, and T. Du. 2013. Partitioning evapotranspiration into soil evaporation and transpiration using a modified dual crop coefficient model in irrigated maize field with ground-mulching. *Agric. Water Manage.* 127:85–96. doi:10.1016/j.agwat.2013.05.018
- Er-Raki, S., A. Chebouni, G. Boulet, and D.G. Williams. 2010. Using the dual approach of FAO-56 for partitioning ET into soil and plant components for olive orchards in a semi-arid region. *Agric. Water Manage.* 97(11):1769–1778. doi:10.1016/j.agwat.2010.06.009
- Fernández, J.E., S.R. Green, H.W. Caspari, A. Diaz-Espejo, and M.V. Cuevas. 2007. The use of sap flow measurements for scheduling irrigation in olive, apple and Asian pear trees and in grapevines. *Plant Soil* 305:91–104. doi:10.1007/s11104-007-9348-8
- Fisher, J.B., D.D. Baldocchi, L. Misson, T.E. Dawson, and A.H. Goldstein. 2007. What the towers don't see at night: Nocturnal sap flow in trees and shrubs at two AmeriFlux sites in California. *Tree Physiol.* 27:597–610. doi:10.1093/treephys/27.4.597
- Folland, C.K., J. Knight, H.W. Linderholm, D. Fereday, S. Ineson, and J.W. Hurrell. 2009. The summer North Atlantic oscillation: Past, present and future. *J. Clim.* 22(5):1082–1103. doi:10.1175/2008JCLI2459.1
- Gayler, S., E. Wang, E. Priesack, T. Schaaf, and F.-X. Maidl. 2002. Modelling biomass growth, N-uptake and phenological development of potato crop. *Geoderma* 105:367–383. doi:10.1016/S0016-7061(01)00113-6
- Godwin, D.C., and C.A. Jones. 1991. Nitrogen dynamics in soil–plant systems. In: J. Hanks and J. Ritchie, editors, *Modeling plant and soil systems.* Agron. Monogr. 31. ASA, CSSA, SSSA, Madison, WI. p. 287–321. doi:10.2134/agronmonogr31.c13
- Hansen, S., H.E. Jensen, N.E. Nielsen, and H. Svendsen. 1990. DAISY—Soil Plant Atmosphere System Model. The Royal Veterinary and Agricultural University, Copenhagen, Denmark.
- Haude, W. 1955. Zur Bestimmung der Verdunstung auf möglichst einfache Weise. *Mitteilungen des Deutschen Wetterdienstes* 11:1–24.
- Herbst, M., W. Fialkiewicz, T. Chen, T. Pütz, D. Thiéry, C. Mouvet, G. Vachaud, and H. Vereecken. 2005. Intercomparison of flow and transport models applied to vertical drainage in cropped lysimeters. *Vadose Zone J.* 4:240–254. doi:10.2136/vzj2004.0070
- Herbst, M., L. Kappen, F. Thamm, and R. Vanselow. 1996. Simultaneous measurements of transpiration, soil evaporation and total evaporation in a maize field in northern Germany. *J. Exp. Bot.* 47(305):1957–1962. doi:10.1093/jxb/47.12.1957
- Huck, M.G., K. Ishihara, C.M. Peterson, and T. Ushijima. 1983. Soybean adaptation to water stress at selected stages of growth. *Plant Physiol.* 73:422–427. doi:10.1104/pp.73.2.422
- Hutson, J.L., and R.J. Wagenet. 1992. LEACHM: Leaching Estimation and Chemistry Model: A process-based model of water and solute movement, transformations, plant uptake and chemical reactions in the unsaturated zone. Version 3.0. Research Ser. 93-3. Cornell Univ., Ithaca, NY.
- Jones, C.A., and J.R. Kiniry. 1986. CERES-Maize: A simulation model of maize growth and development. Texas A&M Univ. Press, Temple, TX.
- Klier, C. 2007. Environmental fate of the herbicide glyphosate in the soil-plant system: Monitoring and modelling using large-scale weighing lysimeters. Technische Universität, Fakultät Wissenschaftszentrum Weihenstephan XVI, München.
- Lawrence, D.M., P.E. Thornton, K.W. Oleson, and G.B. Bonan. 2007. The partitioning of evapotranspiration into transpiration, soil evaporation, and canopy evaporation in a GCM: Impacts on land–atmosphere interaction. *J. Hydrometeorol.* 8:862–880. doi:10.1175/JHM596.1
- Lide, D.R. 1992. Handbook of chemistry and physics. 73rd ed. CRC Press, Inc., Boca Raton, FL. p. 6–10.
- Loos, C., S. Gayler, and E. Priesack. 2007. Assessment of water balance simulations for large-scale weighing lysimeters. *J. Hydrol.* 335:259–270. doi:10.1016/j.jhydrol.2006.11.017
- Madurapperuma, W.S., T.M. Bleby, and S.S.O. Burgess. 2009. Evaluation of sap flow methods to determine water use by cultivated palms. *Environ. Exp. Bot.* 66(3):372–380. doi:10.1016/j.envexpbot.2009.04.002
- Manoli, G., S. Bonetti, E. Scudiero, F. Morari, M. Putti, and P. Teatini. 2015. Modeling soil-plant dynamics: Assessing simulation accuracy by comparison with spatially distributed crop yield measurements. *Vadose Zone J.* 14. doi:10.2136/vzj2015.05.0069
- Marshall, D.C. 1958. Measurement of sap flow in conifers by heat transport. *Plant Physiol.* 33(6):385–396. doi:10.1104/pp.33.6.385
- Milly, P.C.D., K.A. Dunne, and A.V. Vecchia. 2005. Global pattern of trends in streamflow and water availability in a changing climate. *Nature* 438:347–350. doi:10.1038/nature04312
- Mishra, S., and J.C. Parker. 1989. Effects of parameter uncertainty on predictions of unsaturated flow. *J. Hydrol.* 108:19–33.
- Mualem, Y. 1976. A new model for predicting the hydraulic conductivity of unsaturated porous media. *Water Resour. Res.* 12:513–522. doi:10.1029/WR012i003p00513
- Nash, J., and J. Sutcliffe. 1970. River flow forecasting through conceptual models. Part I. A discussion of principles. *J. Hydrol.* 10(3):282–290. doi:10.1016/0022-1694(70)90255-6
- Nimah, M.N., and R.J. Hanks. 1973. Model for estimating soil water, plant, and atmospheric interrelations: I. Description and sensitivity. *Soil Sci. Soc. Am. J.* 37:522–527. doi:10.2136/sssaj1973.03615995003700040018x
- Oliveira, R.S., T.E. Dawson, S.S.O. Burgess, and D.C. Nepstad. 2005. Hydraulic redistribution in three Amazonian trees. *Oecologia* 145:354–363. doi:10.1007/s00442-005-0108-2
- Palmer, T.N., and J. Räisänen. 2002. Quantifying the risk of extreme seasonal precipitation events in a changing climate. *Nature* 415:512–514. doi:10.1038/415512a
- Parton, W.J., D.S. Ojima, C.V. Cole, and D.S. Schimel. 1994. A general model for soil organic matter dynamics: Sensitivity to litter chemistry, texture and management. In: R. Bryant and R. Arnold, editors, *Quantitative modeling of soil forming processes.* SSSA Spec. Publ. 39. SSSA, Madison, WI. p. 147–167. doi:10.2136/sssaspecpub39.c9
- Pfautsch, S., C. Keitel, T.L. Turnbull, M.J. Braimbridge, T.E. Wright, R.R. Simpson, J.A. O'Brien, and M.A. Adams. 2011. Diurnal patterns of water use in *Eucalyptus vitrix* indicate pronounced desiccation-

- rehydration cycles despite unlimited water supply. *Tree Physiol.* 31:1041–1051. doi:10.1093/treephys/tpo082
- Phogat, V., M.A. Skewes, J.W. Cox, J. Alam, G. Grigson, and J. Šimůnek. 2013. Evaluation of water movement and nitrate dynamics in a lysimeter planted with an orange tree. *Agric. Water Manage.* 127:74–84. doi:10.1016/j.agwat.2013.05.017
- Priesack, E., S. Gayler, and H.P. Hartmann. 2006. The impact of crop growth sub-model choice on simulated water and nitrogen balances. *Nutr. Cycl. Agroecosyst.* 75:1–13. doi:10.1007/s10705-006-9006-1
- Reth, S., W. Graf, O. Gefke, H.K. Seidlitz, and J.C. Munch. 2007. Whole-year-round observation of N<sub>2</sub>O profiles in soil: A lysimeter study. *Water Air Soil Pollut. Focus* 8(2):129–137. doi:10.1007/s11267-007-9165-3
- Richards, L.A. 1931. Capillary conduction of fluids through porous mediums. *Physics* 1:318–333. doi:10.1063/1.1745010
- Ritchie, J.T. 1991. Wheat phasic development. In: J. Hanks and J.T. Ritchie, editors, *Modeling plant and soil systems*. Agron. Monogr. 31. ASA, CSSA, SSSA, Madison, WI. p. 31–54. doi:10.2134/agronmonogr31.c3
- Ritchie, J.T., and D.C. Godwin. 1989. CERES Wheat 2.0. Documentation for version 2 of the CERES wheat model. [http://nowlin.css.msu.edu/wheat\\_book/](http://nowlin.css.msu.edu/wheat_book/) (accessed 4 Feb. 2015).
- Ritchie, J.T., D.C. Godwin, and S. Otter-Nacke. 1987. CERES-Wheat—A simulation model of wheat growth and development. Texas A&M Univ. Press, College Station, TX.
- Rochette, P., E. Pattey, R.L. Desjardins, L.M. Dwyer, D.W. Stewart, and P.A. Dube. 1991. Estimation of maize (*Zea mays* L.) canopy conductance by scaling up leaf stomatal conductance. *Agric. For. Meteorol.* 54:241–261. doi:10.1016/0168-1923(91)90008-E
- Rosenzweig, C., and M.L. Parry. 1994. Potential impact of climate change on world food supply. *Nature* 367:133–138. doi:10.1038/367133a0
- Schaap, M.G., F.J. Leij, and M.Th. van Genuchten. 2001. ROSETTA: A computer program for estimating soil hydraulic parameters with hierarchical pedotransfer functions. *J. Hydrol.* 251:163–176. doi:10.1016/S0022-1694(01)00466-8
- Sharp, R.E., and W.J. Davies. 1985. Root growth and water uptake by maize plants in drying soil. *J. Exp. Bot.* 36:1441–1456. doi:10.1093/jxb/36.9.1441
- Šimůnek, J., K. Huang, and M.Th. van Genuchten. 1998. The HYDRUS code for simulating the one-dimensional movement of water, heat, and multiple solutes in variably-saturated media. Version 6.0. Tech. Rep. 144. USDA-ARS, U.S. Salinity Laboratory, Riverside, CA.
- Skaggs, T.H., J.A. Poss, P.J. Shouse, and C.M. Grieve. 2006a. Irrigating forage crops with saline waters: 1. Volumetric lysimeter studies. *Vadose Zone J.* 5:815–823. doi:10.2136/vzj2005.0119
- Skaggs, T.H., P.J. Shouse, and J.A. Poss. 2006b. Irrigating forage crops with saline waters: 2. Modeling root uptake and drainage. *Vadose Zone J.* 5:824–837. doi:10.2136/vzj2005.0120
- Stumpp, C., P. Maloszewski, W. Stichler, and J. Fank. 2009. Environmental isotope ( $\delta^{18}\text{O}$ ) and hydrological data to assess water flow in unsaturated soils planted with different crops: Case study lysimeter station “Wagna” (Austria). *J. Hydrol.* 369:198–208. doi:10.1016/j.jhydrol.2009.02.0047
- Stumpp, C., W. Stichler, M. Kandolf, and J. Šimůnek. 2012. Effects of land cover and fertilization method on water flow and solute transport in five lysimeters: A long-term study using stable water isotopes. *Vadose Zone J.* 11. doi:10.2136/vzj2011.0075
- van Genuchten, M.Th. 1980. A closed-form equation for predicting the hydraulic conductivity of unsaturated soils. *Soil Sci. Soc. Am. J.* 44:892–898. doi:10.2136/sssaj1980.03615995004400050002x
- van Griensven, A., S. Maharjan, and T. Alemayehu. 2014. Improved simulation of evapotranspiration for land use and climate change impact analysis at catchment scale. In: D.P. Ames et al., editors, *Proceedings of the 7th International Congress on Environmental Modelling and Software*, San Diego, CA. p. 2386.
- Walter, I.A., R.G. Allen, R. Elliott, D. Itenfisu, P. Brown, M.E. Jensen, B. Mecham, T.A. Howell, R. Snyder, S. Eching, T. Spofford, M. Hattendorf, D. Martin, R.H. Cuenca, and J.L. Wright. 2005. The ASCE standardized reference evapotranspiration equation. *American Society of Civil Engineers*, Reston, VA. p. 70.
- Wang, E. 1997. Development of a generic process-oriented model for simulation of crop growth. Herberg Utz Verlag, München, Germany. p. 195.
- Wang, E., and T. Engel. 1998. Simulation of phenological development of wheat crops. *Agric. Syst.* 58(1):1–24. doi:10.1016/S0308-521X(98)00028-6
- Wang, E., and T. Engel. 2000. SPASS: A generic process-oriented crop model with versatile windows interface. *Environ. Model. Softw.* 15:179–188. doi:10.1016/S1364-8152(99)00033-X
- Willmott, C.J. 1981. On the validation of models. *Phys. Geogr.* 2:184–194.
- Winkler, J.B., H. Lang, W. Graf, S. Reth, and J.C. Munch. 2009. Experimental setup of field lysimeters for studying effects of elevated ozone and below-ground pathogen infection on a plant-soil-system of juvenile beech (*Fagus sylvatica* L.). *Plant Soil* 323(1–2):7–19. doi:10.1007/s11104-009-9936-x